J Sci Comput
DOI 10.1007/s10915-010-9420-z

A New Class of High-Order Energy Stable Flux Reconstruction Schemes

P.E. Vincent · P. Castonguay · A. Jameson

Received: 2 May 2010 / Revised: 2 September 2010 / Accepted: 5 September 2010

Abstract The flux reconstruction approach to high-order methods is robust, efficient, simple to implement, and allows various high-order schemes, such as the nodal discontinuous Galerkin method and the spectral difference method, to be cast within a single unifying framework. Utilizing a flux reconstruction formulation, it has been proved (for one-dimensional linear advection) that the spectral difference method is stable for all orders of accuracy in a norm of Sobolev type, provided that the interior flux collocation points are located at zeros of the corresponding Legendre polynomials. In this article the aforementioned result is extended in order to develop a new class of one-dimensional energy stable flux reconstruction schemes. The energy stable schemes are parameterized by a single scalar quantity, which if chosen judiciously leads to the recovery of various well known high-order methods (including a particular nodal discontinuous Galerkin method and a particular spectral difference method). The analysis offers significant insight into why certain flux reconstruction schemes are stable, whereas others are not. Also, from a practical standpoint, the analysis provides a simple prescription for implementing an infinite range of energy stable high-order methods via the intuitive flux reconstruction approach.

Keywords High-order methods · Flux reconstruction · Nodal discontinuous Galerkin method · Spectral difference method · Stability

1 Introduction

High-order numerical methods potentially offer better accuracy than low-order schemes for a comparable computational cost. However, existing high-order methods are generally less robust and more complex to implement than their low-order counterparts. These issues, combined with difficulties generating high-order meshes, have prevented the wide-spread adoption of high-order techniques in either academia (where the use of low-order schemes remains widespread) or in industry (where the use of low-order schemes is ubiquitous).

P.E. Vincent (✉) · P. Castonguay · A. Jameson
Department of Aeronautics and Astronautics, Stanford University, Stanford, CA 94305, USA
e-mail: pvincent@stanford.edu

Published online: 17 September 2010

The most mature and widely used high-order methods (at least for unstructured grids) are based on a class of schemes developed in 1973 by Reed and Hill [1] to solve the neutron transport equation. Such schemes have become known as discontinuous Galerkin (DG) methods, and numerous variants have been developed for solving the weak form of both hyperbolic [2] and elliptic systems [3]. The basic principle of DG schemes is to decompose the approximate numerical solution both spatially, by tessellating a given computational domain with separate elements, and also spectrally, via a summation of piecewise discontinuous polynomial basis functions within each element. A particularly simple and efficient range of DG schemes utilize high-order Lagrange polynomial basis functions inside each element, defined by solution values at a set of distinct nodal points. Such schemes have become known as nodal DG methods, an exposition of which can be found in the recent textbook by Hesthaven and Warburton [4], as well as in various articles by the same authors [5, 6]. Similar to nodal DG methods are spectral difference (SD) methods, (although unlike nodal DG methods, SD methods are based on the governing system in its differential form). The foundation for such schemes was first put forward by Kopriva and Kolias [7] in 1996 under the name of "staggered grid Chebyshev multidomain" methods. However, several years later in 2006 Liu, Wang and Vinokular [8] presented a more general formulation for both triangular and quadrilateral elements, which they termed the SD method (a name which has been retained to the present). In recent years a range of studies have successfully employed SD methods to solve a variety of problems [9–11].

The intimate relationship between nodal DG and SD schemes has been clearly highlighted by Huynh, who in 2007 presented the flux reconstruction (FR) approach to high-order methods [12]. Such an approach allows several high-order schemes, including a particular nodal DG method and (for a linear flux function) various SD methods to be cast within a single unifying framework. Furthermore, the FR approach allowed Huynh to create a variety of new high-order schemes with various stability and accuracy properties [12]. In the present article a new class of one-dimensional (1D) energy stable FR schemes is identified. The methodology for developing such schemes is an extension of the approach adopted by Jameson [13], who recently utilized a FR formulation to prove that (for 1D linear advection) the SD method is stable in a norm of Sobolev type, provided that the interior flux collocation points are placed at zeros of the corresponding Legendre polynomials. It is found that all the energy stable FR schemes are parameterized by a single scalar quantity, which if chosen judiciously leads to the recovery of several well known numerical methods (including a particular nodal DG method and a particular SD method), as well as one other FR scheme that was previously found by Huynh to be stable [12].

The article begins with a brief review of the FR approach. Following this review a new class of energy stable FR schemes is identified, and the ability to recover existing schemes (from this class) is demonstrated. Numerical experiments are then performed in order to elucidate various properties of the energy stable schemes. Finally, the extension of such schemes to multiple dimensions is briefly discussed, and conclusions are presented.

2 The Flux Reconstruction Approach to High-Order Methods

2.1 Preliminaries

Consider solving the 1D scalar conservation law

$$\frac{\partial u}{\partial t} + \frac{\partial f}{\partial x} = 0 \tag{2.1}$$

within an arbitrary domain $\mathbf{\Omega}$, where x is a spatial coordinate, t is time, $u = u(x,t)$ is a conserved scalar quantity and $f = f(u)$ is the flux of u in the x direction. Further, consider partitioning $\mathbf{\Omega}$ into N distinct elements each denoted $\mathbf{\Omega}_n = \{x | x_n < x < x_{n+1}\}$ such that

$$\mathbf{\Omega} = \bigcup_{n=0}^{N-1} \mathbf{\Omega}_n, \qquad \bigcap_{n=0}^{N-1} \mathbf{\Omega}_n = \emptyset. \tag{2.2}$$

Finally, having partitioned $\mathbf{\Omega}$ into separate elements, consider representing the exact solution u within each $\mathbf{\Omega}_n$ by a polynomial of degree k denoted $u_n^\delta = u_n^\delta(x,t)$ (which is in general piecewise discontinuous between elements), and the exact flux f within each $\mathbf{\Omega}_n$ by a polynomial of degree $k+1$ denoted $f_n^\delta = f_n^\delta(x,t)$ (which is piecewise continuous between elements), such that a total approximate solution $u^\delta = u^\delta(x,t)$ and a total approximate flux $f^\delta = f^\delta(x,t)$ can be defined within $\mathbf{\Omega}$ as

$$u^\delta = \bigoplus_{n=0}^{N-1} u_n^\delta \approx u, \qquad f^\delta = \bigoplus_{n=0}^{N-1} f_n^\delta \approx f. \tag{2.3}$$

2.2 Implementation

From an implementation perspective, it is advantageous to consider transforming each $\mathbf{\Omega}_n$ to a standard element $\mathbf{\Omega}_S = \{r | -1 \le r \le 1\}$ via the mapping

$$r = \Gamma_n(x) = 2\left(\frac{x - x_n}{x_{n+1} - x_n}\right) - 1, \tag{2.4}$$

which has the inverse

$$x = \Gamma_n^{-1}(r) = \left(\frac{1-r}{2}\right) x_n + \left(\frac{1+r}{2}\right) x_{n+1}. \tag{2.5}$$

Having performed such a transformation, the evolution of u_n^δ within any individual $\mathbf{\Omega}_n$ (and thus the evolution of u^δ within $\mathbf{\Omega}$) can be determined by solving the following transformed equation within the standard element $\mathbf{\Omega}_S$

$$\frac{\partial \hat{u}^\delta}{\partial t} + \frac{\partial \hat{f}^\delta}{\partial r} = 0, \tag{2.6}$$

where

$$\hat{u}^\delta = \hat{u}^\delta(r,t) = u_n^\delta(\Gamma_n^{-1}(r), t) \tag{2.7}$$

is a polynomial of degree k,

$$\hat{f}^\delta = \hat{f}^\delta(r,t) = \frac{f_n^\delta(\Gamma_n^{-1}(r), t)}{J_n} \tag{2.8}$$

is a polynomial of degree $k+1$, and $J_n = (x_{n+1} - x_n)/2$.

The FR approach to solving (2.6) within the standard element $\mathbf{\Omega}_S$ consists of five stages. The first stage is to define a specific form for $\hat{u}^\delta$. To this end, it is assumed that values of $\hat{u}^\delta$

are known at a set of $k+1$ solution points inside $\mathbf{\Omega}_S$, with each point located at a distinct position r_i ($i=0$ to k). Lagrange polynomials $l_i = l_i(r)$ defined as

$$l_i = \prod_{j=0, j\neq i}^{k} \left(\frac{r - r_j}{r_i - r_j} \right) \tag{2.9}$$

can then be used to construct the following expression for $\hat{u}^\delta$

$$\hat{u}^\delta = \sum_{i=0}^{k} \hat{u}_i^\delta l_i, \tag{2.10}$$

where $\hat{u}_i^\delta = \hat{u}_i^\delta(t)$ are the known values of $\hat{u}^\delta$ at the solution points r_i.

The second stage of the FR process involves constructing a degree k polynomial $\hat{f}^{\delta D} = \hat{f}^{\delta D}(r,t)$, defined as the approximate transformed discontinuous flux within $\mathbf{\Omega}_S$. An expression for $\hat{f}^{\delta D}$ can be written as

$$\hat{f}^{\delta D} = \sum_{i=0}^{k} \hat{f}_i^{\delta D} l_i, \tag{2.11}$$

where the coefficients $\hat{f}_i^{\delta D} = \hat{f}_i^{\delta D}(t)$ are simply values of the transformed flux at each solution point r_i evaluated directly from the approximate solution. The flux $\hat{f}^{\delta D}$ is termed discontinuous since it is calculated directly from the approximate solution, which is in general piecewise discontinuous between elements.

The third stage of the FR process involves calculating transformed numerical fluxes at either end of the standard element $\mathbf{\Omega}_S$ (at $r = \pm 1$). In order to calculate such fluxes, one must first obtain values for the approximate solution at either end of the standard element via (2.10). Once obtained, these values can be used in conjunction with analogous information from adjoining elements to calculate transformed numerical interface fluxes. The exact methodology for calculating such numerical fluxes will depend on the nature of the equations being solved. For example, when solving the Euler equations one may use a Roe type approximate Riemann solver [14], or any other two-point flux formula that provides for an upwind bias. In what follows the numerical interface fluxes associated with the left and right hand ends of $\mathbf{\Omega}_S$ (and transformed appropriately for use in $\mathbf{\Omega}_S$) will be denoted $\hat{f}_L^{\delta I}$ and $\hat{f}_R^{\delta I}$ respectively.

The penultimate stage of the FR process involves adding a degree $k+1$ transformed correction flux $\hat{f}^{\delta C} = \hat{f}^{\delta C}(r,t)$ to the approximate transformed discontinuous flux $\hat{f}^{\delta D}$, such that their sum equals the transformed numerical interface flux at $r = \pm 1$, yet follows (in some sense) the approximate discontinuous flux within the interior of $\mathbf{\Omega}_S$. In order to define $\hat{f}^{\delta C}$ such that it satisfies the above requirements, consider first defining degree $k+1$ correction functions $g_L = g_L(r)$ and $g_R = g_R(r)$ that approximate zero (in some sense) within $\mathbf{\Omega}_S$, as well as satisfying

$$g_L(-1) = 1, \qquad g_L(1) = 0, \tag{2.12}$$

$$g_R(-1) = 0, \qquad g_R(1) = 1, \tag{2.13}$$

and based on symmetry considerations

$$g_L(r) = g_R(-r). \tag{2.14}$$

A suitable expression for $\hat{f}^{\delta C}$ can now be written in terms of g_L and g_R as

$$\hat{f}^{\delta C} = (\hat{f}_L^{\delta I} - \hat{f}_L^{\delta D})g_L + (\hat{f}_R^{\delta I} - \hat{f}_R^{\delta D})g_R, \tag{2.15}$$

where $\hat{f}_L^{\delta D} = \hat{f}^{\delta D}(-1,t)$ and $\hat{f}_R^{\delta D} = \hat{f}^{\delta D}(1,t)$. Using this expression, a degree $k+1$ approximate total transformed flux $\hat{f}^{\delta} = \hat{f}^{\delta}(r,t)$ within $\mathbf{\Omega}_S$ can be constructed from the discontinuous and correction fluxes as follows

$$\hat{f}^{\delta} = \hat{f}^{\delta D} + \hat{f}^{\delta C}. \tag{2.16}$$

The final stage of the FR process involves calculating the divergence of $\hat{f}^{\delta}$ at each solution point r_i using the expression

$$\frac{\partial \hat{f}^{\delta}}{\partial r}(r_i) = \sum_{j=0}^{k} \hat{f}_j^{\delta D} \frac{\mathrm{d}l_j}{\mathrm{d}r}(r_i) + (\hat{f}_L^{\delta I} - \hat{f}_L^{\delta D}) \frac{\mathrm{d}g_L}{\mathrm{d}r}(r_i) + (\hat{f}_R^{\delta I} - \hat{f}_R^{\delta D}) \frac{\mathrm{d}g_R}{\mathrm{d}r}(r_i). \tag{2.17}$$

These values can then be used to advance the approximate transformed solution $\hat{u}^{\delta}$ in time via a suitable temporal discretization of the following semi-discrete expression

$$\frac{\partial \hat{u}_i^{\delta}}{\partial t} = -\frac{\partial \hat{f}^{\delta}}{\partial r}(r_i). \tag{2.18}$$

2.3 Comments

The nature of a particular FR scheme depends solely on three factors, namely the location of the solution collocation points r_i, the methodology for calculating the transformed numerical interface fluxes $\hat{f}_L^{\delta I}$ and $\hat{f}_R^{\delta I}$, and finally the form of the flux correction functions g_L (and thus g_R). It has been shown previously that a particular nodal DG scheme is recovered in 1D if the corrections functions g_L and g_R are the right and left Radau polynomials respectively [12]. Specifically, the type of nodal DG scheme recovered involves a collocation projection of the flux onto a polynomial space of degree k; using flux values at the $k+1$ solution points. This aspect of the recovered nodal DG scheme is significant when considering non-linear stability, as will be discussed later. Also, it has been shown that SD type methods can be recovered (at least for a linear flux function) if the corrections g_L and g_R are set to zero at a set of k points within $\mathbf{\Omega}_S$ (located symmetrically about the origin) [12]. Several additional forms of g_L (and thus g_R) have also been suggested, leading to the development of new schemes, with various stability and accuracy properties. For further details of these new schemes see the article by Huynh [12].

3 Identification of Energy Stable Flux Reconstruction Schemes

3.1 Overview

In this section a class of energy stable FR schemes is identified (for 1D linear advection). To begin, various manipulations of the FR formulation are presented, via which criteria are derived that (if satisfied) imply energy stability. This preliminary analysis is based on the recent study of Jameson [13], in which it was proved (for 1D linear advection) that the SD method is stable for all orders of accuracy in a norm of Sobolev type provided that

the interior flux collocation points are placed at the zeros of the corresponding Legendre polynomials. Following identification of the aforementioned stability criteria, a range of flux correction functions (g_L and g_R) are found that lead to energy stable schemes. Finally, the recovery of existing methods from the new class of schemes is demonstrated, and special cases are discussed.

3.2 Preliminaries

Assume that the flux function $f(u)$ introduced in Sect. 2.1 is linear (*i.e.* assume that $f(u) = au$, where a is a constant scalar). Under such an assumption (2.18) can be written as

$$\frac{\mathrm{d}\hat{u}_i^\delta}{\mathrm{d}t} = -\hat{a}\sum_{j=0}^{k}\hat{u}_j^\delta\frac{\mathrm{d}l_j}{\mathrm{d}r}(r_i) - (\hat{f}_L^{\delta I} - \hat{a}\hat{u}_L^\delta)\frac{\mathrm{d}g_L}{\mathrm{d}r}(r_i) - (\hat{f}_R^{\delta I} - \hat{a}\hat{u}_R^\delta)\frac{\mathrm{d}g_R}{\mathrm{d}r}(r_i), \tag{3.1}$$

where $\hat{a} = a/J_n$, $\hat{u}_L^\delta = \hat{u}^\delta(-1,t)$ and $\hat{u}_R^\delta = \hat{u}^\delta(1,t)$. On multiplying (3.1) by a Lagrange polynomial l_i and summing over i (from $i=0$ to $i=k$) one obtains

$$\begin{aligned}\sum_{i=0}^{k}\frac{\mathrm{d}\hat{u}_i^\delta}{\mathrm{d}t}l_i = -\hat{a}\sum_{i=0}^{k}\sum_{j=0}^{k}\hat{u}_j^\delta\frac{\mathrm{d}l_j}{\mathrm{d}r}(r_i)l_i \\ - (\hat{f}_L^{\delta I} - \hat{a}\hat{u}_L^\delta)\sum_{i=0}^{k}\frac{\mathrm{d}g_L}{\mathrm{d}r}(r_i)l_i - (\hat{f}_R^{\delta I} - \hat{a}\hat{u}_R^\delta)\sum_{i=0}^{k}\frac{\mathrm{d}g_R}{\mathrm{d}r}(r_i)l_i,\end{aligned} \tag{3.2}$$

and thus

$$\frac{\partial\hat{u}^\delta}{\partial t} = -\hat{a}\frac{\partial\hat{u}^\delta}{\partial r} - (\hat{f}_L^{\delta I} - \hat{a}\hat{u}_L^\delta)\frac{\mathrm{d}g_L}{\mathrm{d}r} - (\hat{f}_R^{\delta I} - \hat{a}\hat{u}_R^\delta)\frac{\mathrm{d}g_R}{\mathrm{d}r}. \tag{3.3}$$

On differentiating (3.3) k times (in space) one obtains

$$\frac{\partial}{\partial t}\left(\frac{\partial^k\hat{u}^\delta}{\partial r^k}\right) = -\hat{a}\frac{\partial^{k+1}\hat{u}^\delta}{\partial r^{k+1}} - (\hat{f}_L^{\delta I} - \hat{a}\hat{u}_L^\delta)\frac{\mathrm{d}^{k+1}g_L}{\mathrm{d}r^{k+1}} - (\hat{f}_R^{\delta I} - \hat{a}\hat{u}_R^\delta)\frac{\mathrm{d}^{k+1}g_R}{\mathrm{d}r^{k+1}}, \tag{3.4}$$

where it can be noted that since $\hat{u}^\delta$ is a polynomial of degree k

$$\frac{\partial^{k+1}\hat{u}^\delta}{\partial r^{k+1}} = 0, \tag{3.5}$$

and thus

$$\frac{\partial}{\partial t}\left(\frac{\partial^k\hat{u}^\delta}{\partial r^k}\right) = -(\hat{f}_L^{\delta I} - \hat{a}\hat{u}_L^\delta)\frac{\mathrm{d}^{k+1}g_L}{\mathrm{d}r^{k+1}} - (\hat{f}_R^{\delta I} - \hat{a}\hat{u}_R^\delta)\frac{\mathrm{d}^{k+1}g_R}{\mathrm{d}r^{k+1}}. \tag{3.6}$$

On multiplying (3.3) by the approximate transformed solution $\hat{u}^\delta$ and integrating over $\mathbf{\Omega}_S$ one obtains

$$\begin{aligned}\int_{-1}^{1}\hat{u}^\delta\frac{\partial\hat{u}^\delta}{\partial t}\mathrm{d}r = -\hat{a}\int_{-1}^{1}\hat{u}^\delta\frac{\partial\hat{u}^\delta}{\partial r}\mathrm{d}r - (\hat{f}_L^{\delta I} - \hat{a}\hat{u}_L^\delta)\int_{-1}^{1}\hat{u}^\delta\frac{\mathrm{d}g_L}{\mathrm{d}r}\mathrm{d}r \\ - (\hat{f}_R^{\delta I} - \hat{a}\hat{u}_R^\delta)\int_{-1}^{1}\hat{u}^\delta\frac{\mathrm{d}g_R}{\mathrm{d}r}\mathrm{d}r,\end{aligned} \tag{3.7}$$

and thus by parts

$$\frac{\mathrm{d}}{\mathrm{d}t}\int_{-1}^{1}(\hat{u}^{\delta})^2\mathrm{d}r = -\hat{a}[(\hat{u}_R^{\delta})^2-(\hat{u}_L^{\delta})^2] - 2(\hat{f}_L^{\delta I}-\hat{a}\hat{u}_L^{\delta})\left(-\hat{u}_L^{\delta}-\int_{-1}^{1}g_L\frac{\partial\hat{u}^{\delta}}{\partial r}\mathrm{d}r\right) - 2(\hat{f}_R^{\delta I}-\hat{a}\hat{u}_R^{\delta})\left(\hat{u}_R^{\delta}-\int_{-1}^{1}g_R\frac{\partial\hat{u}^{\delta}}{\partial r}\mathrm{d}r\right). \tag{3.8}$$

On multiplying (3.6) by the kth derivative of the approximate transformed solution $\hat{u}^{\delta}$ and integrating over $\boldsymbol{\Omega}_S$ one obtains

$$\int_{-1}^{1}\left(\frac{\partial^k\hat{u}^{\delta}}{\partial r^k}\right)\frac{\partial}{\partial t}\left(\frac{\partial^k\hat{u}^{\delta}}{\partial r^k}\right)\mathrm{d}r = -(\hat{f}_L^{\delta I}-\hat{a}\hat{u}_L^{\delta})\int_{-1}^{1}\left(\frac{\partial^k\hat{u}^{\delta}}{\partial r^k}\right)\left(\frac{\mathrm{d}l^{k+1}g_L}{\mathrm{d}r^{k+1}}\right)\mathrm{d}r - (\hat{f}_R^{\delta I}-\hat{a}\hat{u}_R^{\delta})\int_{-1}^{1}\left(\frac{\partial^k\hat{u}^{\delta}}{\partial r^k}\right)\left(\frac{\mathrm{d}^{k+1}g_R}{\mathrm{d}r^{k+1}}\right)\mathrm{d}r, \tag{3.9}$$

and thus since $\hat{u}^{\delta}$ is a polynomial of degree k, and g_L and g_R are polynomials of degree $k+1$

$$\frac{1}{2}\frac{\mathrm{d}}{\mathrm{d}t}\int_{-1}^{1}\left(\frac{\partial^k\hat{u}^{\delta}}{\partial r^k}\right)^2\mathrm{d}r = -2(\hat{f}_L^{\delta I}-\hat{a}\hat{u}_L^{\delta})\left(\frac{\partial^k\hat{u}^{\delta}}{\partial r^k}\right)\left(\frac{\mathrm{d}^{k+1}g_L}{\mathrm{d}r^{k+1}}\right) - 2(\hat{f}_R^{\delta I}-\hat{a}\hat{u}_R^{\delta})\left(\frac{\partial^k\hat{u}^{\delta}}{\partial r^k}\right)\left(\frac{\mathrm{d}^{k+1}g_R}{\mathrm{d}r^{k+1}}\right). \tag{3.10}$$

On multiplying (3.10) by an as yet undefined scalar quantity c, and summing with (3.8), one obtains

$$\begin{aligned}&\frac{\mathrm{d}}{\mathrm{d}t}\int_{-1}^{1}(\hat{u}^{\delta})^2+\frac{c}{2}\left(\frac{\partial^k\hat{u}^{\delta}}{\partial r^k}\right)^2\mathrm{d}r\\ &= -\hat{a}[(\hat{u}_R^{\delta})^2-(\hat{u}_L^{\delta})^2]-2(\hat{f}_L^{\delta I}-\hat{a}\hat{u}_L^{\delta})\left[-\hat{u}_L^{\delta}-\int_{-1}^{1}g_L\frac{\partial\hat{u}^{\delta}}{\partial r}\mathrm{d}r+c\left(\frac{\partial^k\hat{u}^{\delta}}{\partial r^k}\right)\left(\frac{\mathrm{d}^{k+1}g_L}{\mathrm{d}r^{k+1}}\right)\right]\\ &\quad -2(\hat{f}_R^{\delta I}-\hat{a}\hat{u}_R^{\delta})\left[\hat{u}_R^{\delta}-\int_{-1}^{1}g_R\frac{\partial\hat{u}^{\delta}}{\partial r}\mathrm{d}r+c\left(\frac{\partial^k\hat{u}^{\delta}}{\partial r^k}\right)\left(\frac{\mathrm{d}^{k+1}g_R}{\mathrm{d}r^{k+1}}\right)\right].\end{aligned} \tag{3.11}$$

If it is required that

$$\int_{-1}^{1}g_L\frac{\partial\hat{u}^{\delta}}{\partial r}\mathrm{d}r - c\left(\frac{\partial^k\hat{u}^{\delta}}{\partial r^k}\right)\left(\frac{\mathrm{d}^{k+1}g_L}{\mathrm{d}r^{k+1}}\right)=0, \tag{3.12}$$

and

$$\int_{-1}^{1}g_R\frac{\partial\hat{u}^{\delta}}{\partial r}\mathrm{d}r - c\left(\frac{\partial^k\hat{u}^{\delta}}{\partial r^k}\right)\left(\frac{\mathrm{d}^{k+1}g_R}{\mathrm{d}r^{k+1}}\right)=0, \tag{3.13}$$

(exactly how such requirements can be satisfied will be discussed shortly), then (3.11) can be written as

$$\frac{\mathrm{d}}{\mathrm{d}t}\int_{-1}^{1}(\hat{u}^{\delta})^2+\frac{c}{2}\left(\frac{\partial^k\hat{u}^{\delta}}{\partial r^k}\right)^2\mathrm{d}r = (2\hat{f}_L^{\delta I}-\hat{a}\hat{u}_L^{\delta})\hat{u}_L^{\delta}-(2\hat{f}_R^{\delta I}-\hat{a}\hat{u}_R^{\delta})\hat{u}_R^{\delta}. \tag{3.14}$$

Finally, on transforming (3.14) back to the physical space element $\mathbf{\Omega}_n$ one obtains

$$\frac{\mathrm{d}}{\mathrm{d}t}\int_{x_n}^{x_{n+1}}(u_n^{\delta})^2+\frac{c}{2}(J_n)^{2k}\left(\frac{\partial^k u_n^{\delta}}{\partial x^k}\right)^2\mathrm{d}x = [2f_n^{\delta I}-au_n^{\delta}(x_n)]u_n^{\delta}(x_n)-[2f_{n+1}^{\delta I}-au_n^{\delta}(x_{n+1})]u_n^{\delta}(x_{n+1}), \tag{3.15}$$

where $f_n^{\delta I}$ and $f_{n+1}^{\delta I}$ are numerical interface fluxes in physical space evaluated at x_n and x_{n+1} respectively. If the numerical flux at each internal interface x_n $(1\le n\le N-1)$ is defined to have the form

$$f_n^{\delta I}=a\left[\frac{u_n^{\delta}(x_n)+u_{n-1}^{\delta}(x_n)}{2}\right]-|a|(1-\kappa)\left[\frac{u_n^{\delta}(x_n)-u_{n-1}^{\delta}(x_n)}{2}\right], \tag{3.16}$$

where $0\le\kappa\le 1$ (with $\kappa=0$ recovering a fully upwind scheme, and $\kappa=1$ recovering a central scheme), and if for simplicity the domain $\mathbf{\Omega}$ is assumed to be periodic such that

$$f_0^{\delta I}=f_N^{\delta I}=a\left[\frac{u_0^{\delta}(x_0)+u_{N-1}^{\delta}(x_N)}{2}\right]-|a|(1-\kappa)\left[\frac{u_0^{\delta}(x_0)-u_{N-1}^{\delta}(x_N)}{2}\right], \tag{3.17}$$

then summing (3.15) over all elements one obtains

$$\frac{\mathrm{d}}{\mathrm{d}t}\|u^{\delta}\|_{k,2}^2=-\sum_{n=0}^{N-2}|a|(1-\kappa)[u_{n+1}^{\delta}(x_{n+1})-u_n^{\delta}(x_{n+1})]^2 - |a|(1-\kappa)[u_0^{\delta}(x_0)-u_{N-1}^{\delta}(x_N)]^2, \tag{3.18}$$

where

$$\|u^{\delta}\|_{k,2}=\left[\sum_{n=0}^{N-1}\int_{x_n}^{x_{n+1}}(u_n^{\delta})^2+\frac{c}{2}(J_n)^{2k}\left(\frac{\partial^k u_n^{\delta}}{\partial x^k}\right)^2\mathrm{d}x\right]^{1/2}. \tag{3.19}$$

Therefore, since $0\le\kappa\le 1$, it can be concluded that

$$\frac{\mathrm{d}}{\mathrm{d}t}\|u^{\delta}\|_{k,2}^2\le 0, \tag{3.20}$$

where equality with zero is achieved if a central flux is chosen ($\kappa=1$). It can be noted that $\|u^{\delta}\|_{k,2}$ has the form of a broken Sobolev norm.

3.3 Criteria for Stability

Equation (3.20) implies energy stability provided that one can guarantee $\|u^{\delta}\|_{k,2}$ is indeed a norm. Specifically, this amounts to ensuring that $0<\|u^{\delta}\|_{k,2}^2<\infty$ when u^{δ} is finite. For

Table 1 Values of $c_-(k)$ for $2 \le k \le 5$

k	$c_-(k)$
2	$-2/45$
3	$-2/1575$
4	$-2/99225$
5	$-2/9823275$

such a condition to be satisfied, one must be able to guarantee that

$$0 < \int_{x_n}^{x_{n+1}} (u_n^\delta)^2 + \frac{c}{2}(J_n)^{2k} \left(\frac{\partial^k u_n^\delta}{\partial x^k} \right)^2 \mathrm{d}x < \infty \tag{3.21}$$

within each element $\mathbf{\Omega}_n$, and thus

$$0 < \int_{-1}^{1} (\hat{u}^\delta)^2 + \frac{c}{2} \left(\frac{\partial^k \hat{u}^\delta}{\partial r^k} \right)^2 \mathrm{d}r < \infty \tag{3.22}$$

within the standard element $\mathbf{\Omega}_S$. To understand how (3.22) can be satisfied, consider expanding $\hat{u}^\delta$ in terms of Legendre polynomials L_i as follows

$$\hat{u}^\delta = \sum_{i=0}^{k} \phi_i L_i, \tag{3.23}$$

where $\phi_i = \phi_i(t)$ are expansion coefficients. On substituting (3.23) into (3.22) one obtains

$$0 < \sum_{i=0}^{k} \left(\frac{2}{2i+1} \right) \phi_i^2 + c(a_k k!)^2 \phi_k^2 < \infty, \tag{3.24}$$

where a_k is the coefficient of the leading monomial term in the Legendre polynomial L_k, defined as

$$a_k = \frac{(2k)!}{2^k (k!)^2}. \tag{3.25}$$

Manipulation of (3.24) leads to

$$0 < \sum_{i=0}^{k-1} \left(\frac{2}{2i+1} \right) \phi_i^2 + \left[\left(\frac{2}{2k+1} \right) + c(a_k k!)^2 \right] \phi_k^2 < \infty, \tag{3.26}$$

which is guaranteed to be satisfied for finite u^δ provided

$$c_-(k) < c < \infty, \tag{3.27}$$

where

$$c_-(k) = \frac{-2}{(2k+1)(a_k k!)^2}. \tag{3.28}$$

Values of $c_-(k)$ for $2 \le k \le 5$ are listed in Table 1.

Having identified a range for c such that $\|u^\delta\|_{k,2}$ is indeed a norm, we can now state clearly all requirements that must be satisfied to ensure stability. Specifically:

- Equations (3.12) and (3.13) must be satisfied to ensure (3.20) is valid.
- The parameter c must lie within the range defined by (3.27). This ensures that $\|u^\delta\|_{k,2}$ is a indeed norm, which is necessary if one is to infer from (3.20) that the solution is bounded in $\|u^\delta\|_{k,2}$ (and thus in any norm due to equivalence of norms in a finite dimensional space).

Any correction functions g_L and g_R which satisfy (3.12) and (3.13) for a value of c within the range defined by (3.27) can be used to construct energy stable FR schemes.

3.4 Identification of Suitable Flux Correction Functions g_L and g_R

The objective of the following analysis is to identify correction functions g_L and g_R (in terms of the parameter c) such that (3.12) and (3.13) are satisfied. Such functions will lead to energy stable FR schemes provided c lies within the range defined by (3.27).

To begin, consider substituting (2.10) into (3.12) and (3.13), thus obtaining

$$\sum_{i=0}^{k} \hat{u}_i^\delta \left[\int_{-1}^{1} g_L \frac{\mathrm{d}l_i}{\mathrm{d}r} \mathrm{d}r - c \left(\frac{\mathrm{d}^k l_i}{\mathrm{d}r^k} \right) \left(\frac{\mathrm{d}^{k+1} g_L}{\mathrm{d}r^{k+1}} \right) \right] = 0, \tag{3.29}$$

and

$$\sum_{i=0}^{k} \hat{u}_i^\delta \left[\int_{-1}^{1} g_R \frac{\mathrm{d}l_i}{\mathrm{d}r} \mathrm{d}r - c \left(\frac{\mathrm{d}^k l_i}{\mathrm{d}r^k} \right) \left(\frac{\mathrm{d}^{k+1} g_R}{\mathrm{d}r^{k+1}} \right) \right] = 0, \tag{3.30}$$

which can be satisfied independently of the transformed solution (defined by the coefficients $\hat{u}_i^\delta$) provided

$$\int_{-1}^{1} g_L \frac{\mathrm{d}l_i}{\mathrm{d}r} \mathrm{d}r - c \left(\frac{\mathrm{d}^k l_i}{\mathrm{d}r^k} \right) \left(\frac{\mathrm{d}^{k+1} g_L}{\mathrm{d}r^{k+1}} \right) = 0 \quad \forall i, \tag{3.31}$$

and

$$\int_{-1}^{1} g_R \frac{\mathrm{d}l_i}{\mathrm{d}r} \mathrm{d}r - c \left(\frac{\mathrm{d}^k l_i}{\mathrm{d}r^k} \right) \left(\frac{\mathrm{d}^{k+1} g_R}{\mathrm{d}r^{k+1}} \right) = 0 \quad \forall i. \tag{3.32}$$

It has previously been stated that $g_L(r) = g_R(-r)$ (due to symmetry considerations). If this condition is combined with the assumption that the solution points r_i, used to define the nodal basis functions l_i, are symmetric about $r = 0$, then (3.31) and (3.32) collapse to the single requirement that

$$\int_{-1}^{1} g_L \frac{\mathrm{d}l_i}{\mathrm{d}r} \mathrm{d}r - c \left(\frac{\mathrm{d}^k l_i}{\mathrm{d}r^k} \right) \left(\frac{\mathrm{d}^{k+1} g_L}{\mathrm{d}r^{k+1}} \right) = 0 \quad \forall i, \tag{3.33}$$

with g_R obtained via $g_L(r) = g_r(-r)$.

In order to elucidate exactly how (3.33) can be satisfied, consider expanding each Lagrange polynomial l_i in terms of a monomial basis as follows

$$l_i = \sum_{j=0}^{k} \zeta_{ij} r^j, \tag{3.34}$$

where ζ_{ij} are expansion coefficients. On substituting (3.34) into (3.33) one obtains

$$\sum_{j=0}^{k} j\zeta_{ij}\int_{-1}^{1} r^{j-1}g_L \mathrm{d}r - ck!\zeta_{ik}\left(\frac{\mathrm{d}^{k+1}g_L}{\mathrm{d}r^{k+1}}\right) = 0 \quad \forall i, \tag{3.35}$$

and thus

$$\left[\sum_{j=0}^{k-1} j\left(\frac{\zeta_{ij}}{\zeta_{ik}}\right)\int_{-1}^{1} r^{j-1}g_L \mathrm{d}r\right] + k\int_{-1}^{1} r^{k-1}g_L \,\mathrm{d}r - ck!\left(\frac{\mathrm{d}^{k+1}g_L}{\mathrm{d}r^{k+1}}\right) = 0 \quad \forall i, \tag{3.36}$$

which is satisfied independently of the solution basis if it is required that

$$\int_{-1}^{1} r^j g_L \,\mathrm{d}r = \begin{cases} 0 & 0 \le j \le k-2 \\ \dfrac{ck!}{k}\left(\dfrac{\mathrm{d}^{k+1}g_L}{\mathrm{d}r^{k+1}}\right) & j = k-1. \end{cases} \tag{3.37}$$

In order to find solutions to (3.37), consider expanding g_L in terms of Legendre polynomials L_l as follows

$$g_L = \sum_{l=0}^{k+1} \psi_l L_l, \tag{3.38}$$

where ψ_l are expansion coefficients. On substituting (3.38) into (3.37), and using the orthogonality property of Legendre polynomials, one finds that $\psi_l = 0$ for $0 \le l \le k-2$, and

$$\psi_{k-1} = \frac{ck!(k+1)!a_{k+1}\psi_{k+1}}{k\int_{-1}^{1} r^{k-1}L_{k-1}\mathrm{d}r}, \tag{3.39}$$

which using

$$\int_{-1}^{1} r^{k-1}L_{k-1}\mathrm{d}r = \frac{1}{a_{k-1}}\int_{-1}^{1} L_{k-1}L_{k-1}\mathrm{d}r = \frac{2}{(2k-1)a_{k-1}} = \frac{2}{ka_k} \tag{3.40}$$

can be written as

$$\psi_{k-1} = \left(\frac{ck!(k+1)!a_{k+1}a_k}{2}\right)\psi_{k+1} = \left(\frac{c(2k+1)(a_k k!)^2}{2}\right)\psi_{k+1}. \tag{3.41}$$

At this stage of the analysis $k-1$ of the coefficients used to define g_L are known (specifically $\psi_l = 0$ for $0 \le l \le k-2$), and one expression is available to define the remaining three coefficients (ψ_{k-1}, ψ_k and ψ_{k+1}). Clearly two more expressions are required in order to fully define g_L. These can be obtained from the end point conditions defined by (2.12). Specifically, consider substituting (3.38) into (2.12). Using the fact that $\psi_l = 0$ for $0 \le l \le k-2$, one obtains

$$\psi_{k-1} - \psi_k + \psi_{k+1} = (-1)^{k+1}, \tag{3.42}$$

and

$$\psi_{k-1} + \psi_k + \psi_{k+1} = 0. \tag{3.43}$$

Equations (3.41), (3.42) and (3.43) can now be solved to obtain

$$\psi_{k-1} = \frac{\eta_k(-1)^{k+1}}{2(1+\eta_k)}, \qquad \psi_k = \frac{(-1)^k}{2}, \qquad \psi_{k+1} = \frac{(-1)^{k+1}}{2(1+\eta_k)}, \tag{3.44}$$

where

$$\eta_k = \frac{c(2k+1)(a_k k!)^2}{2}. \tag{3.45}$$

Therefore g_L can be written as

$$g_L = \frac{(-1)^k}{2}\left[L_k - \left(\frac{\eta_k L_{k-1} + L_{k+1}}{1+\eta_k}\right)\right], \tag{3.46}$$

and by symmetry g_R can be written as

$$g_R = \frac{1}{2}\left[L_k + \left(\frac{\eta_k L_{k-1} + L_{k+1}}{1+\eta_k}\right)\right], \tag{3.47}$$

where k is the order of the solution polynomial within each element.

Use of correction functions defined by (3.46) and (3.47) will result in energy stable FR schemes provided c lies within the range defined by (3.27). It can be noted that other than the requirement of symmetric solution points, energy stability of the schemes is independent of the solution basis.

3.5 Recovery of Existing Schemes

3.5.1 Nodal Discontinuous Galerkin Scheme

If $c = 0$, then $\eta_k = 0$ which implies

$$g_L = \frac{(-1)^k}{2}(L_k - L_{k+1}), \tag{3.48}$$

and

$$g_R = \frac{1}{2}(L_k + L_{k+1}). \tag{3.49}$$

These can be recognized as expressions for the right and left Radau polynomials respectively. Thus, following the analysis of Huynh [12], a particular nodal DG scheme is recovered. As has been mentioned previously, the recovered scheme involves a collocation projection of the flux onto a polynomial space of degree k; using flux values at the $k+1$ solution points. This aspect of the recovered scheme is significant when considering nonlinear stability, as will be discussed later. Plots of g_L associated with $c = 0$ are shown in Fig. 1 for $2 \leq k \leq 5$.

3.5.2 Spectral Difference Scheme

In order to reproduce a SD scheme (at least for a linear flux function) one must be able to guarantee that the total correction flux $\hat{f}^{\delta C}$ is zero at a set of k points internal to the standard element $\mathbf{\Omega}_S$ [12]. To satisfy such a requirement it is necessary that the left and right correction functions (g_L and g_R respectively) have coincident zeros; which is equivalent to

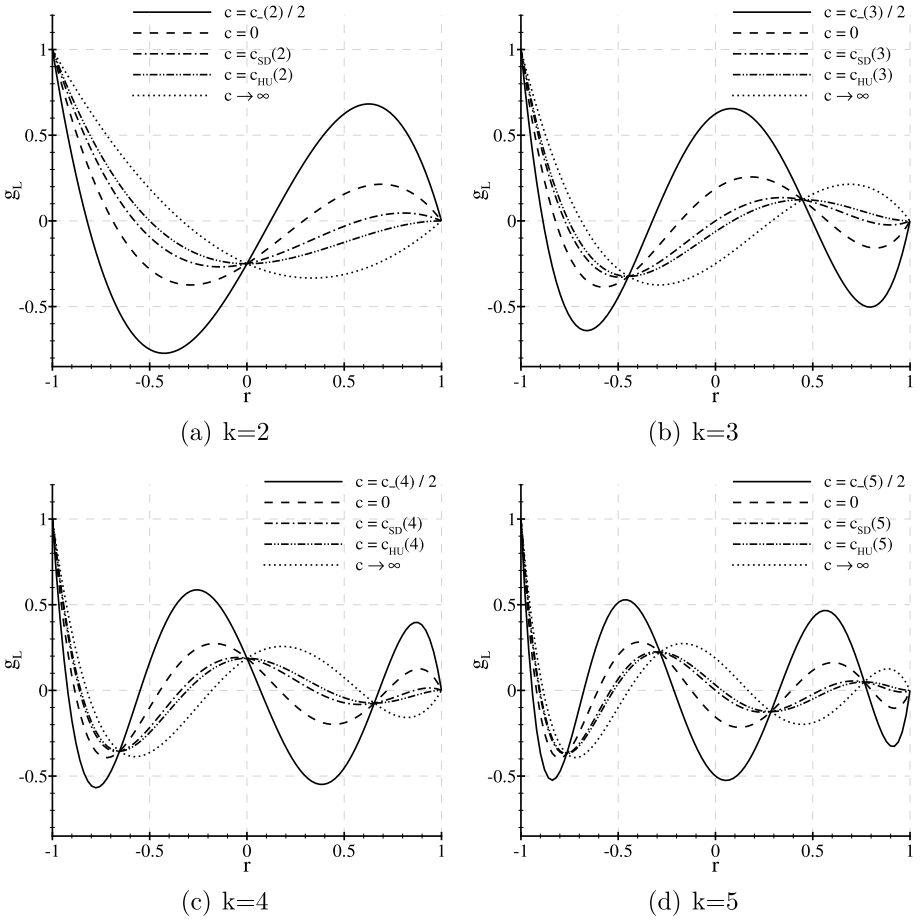

Fig. 1 Plots of the correction function g_L when $k = 2$ (**a**), $k = 3$ (**b**), $k = 4$ (**c**), and $k = 5$ (**d**), for various values of c

requiring symmetrically located zeros (about $r = 0$), since it has previously been stated that $g_L(r) = g_R(-r)$. The only way in which such a requirement can be satisfied is if $c = c_{SD}(k)$ where

$$c_{SD}(k) = \frac{2k}{(2k+1)(k+1)(a_k k!)^2}. \tag{3.50}$$

This leads to

$$\eta_k = \frac{k}{k+1}, \tag{3.51}$$

which implies

$$g_L = \frac{(-1)^k}{2}\left[L_k - \left(\frac{kL_{k-1} + (k+1)L_{k+1}}{2k+1}\right)\right] = \frac{(-1)^k}{2}(1-x)L_k, \tag{3.52}$$

Table 2 Values of $c_{SD}(k)$ for $2 \leq k \leq 5$

k	$c_{SD}(k)$
2	4/135
3	1/1050
4	8/496125
5	1/5893965

and

$$g_R = \frac{1}{2}\left[L_k + \left(\frac{kL_{k-1} + (k+1)L_{k+1}}{2k+1}\right)\right] = \frac{1}{2}(1+x)L_k, \tag{3.53}$$

both of which have k symmetrically located (and hence coincident) zeros internal to $\mathbf{\Omega}_S$. Values of $c_{SD}(k)$ for $2 \leq k \leq 5$ are listed in Table 2, and plots of g_L associated with $c = c_{SD}(k)$ for $2 \leq k \leq 5$ are shown in Fig. 1.

It can be noted that the recovered SD method is identical to the scheme that Jameson [13] proved to be stable (the interior flux collocation points are at zeros of the Legendre polynomial of degree k). It can also be noted that the recovered SD method is identical to the only SD type scheme that Huynh found to be devoid of weak instabilities [12].

3.5.3 Huynh Type Scheme

In the original presentation of the FR approach by Huynh [12] a range of methods were investigated (in addition to DG and SD type schemes). One of these additional methods, which Huynh denoted the g_2 method, proved to be particularly stable. It is found that such a scheme can be recovered if one sets $c = c_{HU}(k)$ where

$$c_{HU}(k) = \frac{2(k+1)}{(2k+1)k(a_k k!)^2}. \tag{3.54}$$

This leads to

$$\eta_k = \frac{k+1}{k}, \tag{3.55}$$

which implies

$$g_L = \frac{(-1)^k}{2}\left[L_k - \left(\frac{(k+1)L_{k-1} + kL_{k+1}}{2k+1}\right)\right], \tag{3.56}$$

and

$$g_R = \frac{1}{2}\left[L_k + \left(\frac{(k+1)L_{k-1} + kL_{k+1}}{2k+1}\right)\right]. \tag{3.57}$$

These expressions are consistent with those derived by Huynh for the g_2 method. Values of $c_{HU}(k)$ for $2 \leq k \leq 5$ are listed in Table 3, and plots of g_L associated with $c = c_{HU}(k)$ for $2 \leq k \leq 5$ are shown in Fig. 1.

3.6 Special Cases

As well as recovering known methods, it is also useful to highlight the behavior of g_L and g_R as c approaches the bounds defined by (3.27). The first case to consider is the behavior

Table 3 Values of $c_{HU}(k)$ for $2 \leq k \leq 5$

k	$c_{HU}(k)$
2	1/15
3	8/4725
4	1/39690
5	12/49116375

of g_L and g_R in the limit $c \to c_-(k)$. This leads to $\eta_k \to -1$, which implies g_L and g_R both tend to infinity. Clearly constructing schemes in the limit $c \to c_-(k)$ is not viable.

The second case to consider is the behavior of g_L and g_R in the limit $c \to \infty$. This leads to $\eta_k \to \infty$, which implies

$$g_L = \frac{(-1)^{k-1}}{2}(L_{k-1} - L_k), \tag{3.58}$$

and

$$g_R = \frac{1}{2}(L_{k-1} + L_k). \tag{3.59}$$

There are three points of note regarding these expressions for g_L and g_R. The first is simply that they exist, and thus $c \to \infty$ results in a viable scheme. The second is that (3.58) and (3.59) can be recognized as expressions for the right and left Radau polynomials (respectively) of one degree less than those which recover a DG scheme. The final point is that in the limit $c \to \infty$, g_L and g_R (and thus the total approximate transformed flux $\hat{f}^\delta$) become polynomials of degree k (the same degree as the approximate transformed solution $\hat{u}^\delta$). To gain insight into the implications of this behavior, consider expanding $\hat{u}^\delta$ within $\mathbf{\Omega}_S$ in terms of a monomial basis as

$$\hat{u}^\delta = \sum_{i=0}^{k} \beta_i r^i, \tag{3.60}$$

where $\beta_i = \beta_i(t)$ are expansion coefficients. Also (in the limit $c \to \infty$) consider expanding $\hat{f}^\delta$ within $\mathbf{\Omega}_S$ in terms of a monomial basis as

$$\hat{f}^\delta = \sum_{i=0}^{k} \chi_i r^i, \tag{3.61}$$

where $\chi_i = \chi_i(t)$ are expansion coefficients, and it is noted that since $c \to \infty$, $\hat{f}^\delta$ is of degree k. Substitution of (3.60) and (3.61) into (2.6) (the general governing equation for the transformed approximate solution within $\mathbf{\Omega}_S$) leads to

$$\sum_{i=0}^{k} \left(\frac{\partial \beta_i}{\partial t} r^i + i\, \chi_i r^{i-1} \right) = 0. \tag{3.62}$$

On multiplication of (3.62) by a Legendre polynomial L_j and integration over $\mathbf{\Omega}_S$ one obtains

$$\sum_{i=0}^{k} \left(\frac{\partial \beta_i}{\partial t} \int_{-1}^{1} r^i L_j \mathrm{d}r + i\, \chi_i \int_{-1}^{1} r^{i-1} L_j \mathrm{d}r \right) = 0, \tag{3.63}$$

which for j in the range $0 \leq j \leq k$ leads (in general) to

$$\frac{\partial \beta_j}{\partial t} = \begin{cases} \neq 0 & 0 \leq j \leq k-1 \\ = 0 & j = k. \end{cases} \tag{3.64}$$

This suggests that in the limit $c \to \infty$, the energy of the highest order term in the expansion of the approximate transformed solution $\hat{u}^{\delta}$ will remain constant; fixed at its initial value.

Plots of g_L associated with $c = c_-(k)/2$ and $c \to \infty$ are shown in Fig. 1 for $2 \leq k \leq 5$.

4 Numerical Experiments

4.1 Linear Flux

4.1.1 Overview

A range of numerical experiments were undertaken in which (2.1) was solved with the following linear flux function

$$f(x,t) = u(x,t). \tag{4.1}$$

For all experiments the computational domain was defined to be $\mathbf{\Omega} = [-1, 1]$. Cases in which a fully upwind flux was prescribed between adjoining elements were considered, as well as cases in which a central flux was prescribed between adjoining elements. In all cases $\mathbf{\Omega}$ was subdivided into ten elements of equal size, and the solution within each element was represented by a third order polynomial, defined by solution values at four Gauss-Lobatto points. Periodic boundary conditions were applied at the ends of $\mathbf{\Omega}$, and the following Gaussian profile was prescribed within $\mathbf{\Omega}$ at $t = 0$

$$u(x,0) = e^{-20x^2}. \tag{4.2}$$

Time integration was performed using an explicit five-stage low storage fourth-order Runge-Kutta scheme [15].

4.1.2 Results (Fully Upwind Flux)

Plots of the solution at time $t = 20$ (for the case of a fully upwind interface flux) are presented in Fig. 2 for various values of c. The most accurate result is achieved when $c = 0$ (recovering a nodal DG scheme). When $c = c_-(3)/2$ oscillations are observed to form predominantly downwind of the Gaussian profile, and when $c = c_{SD}(3)$ and $c = c_{HU}(3)$ oscillations are observed to form predominantly upwind of the Gaussian profile. In the limit $c \to \infty$ a significant loss of accuracy is observed.

Plots illustrating how the L^2 energy of the solution varies with time (for the case of a fully upwind interface flux) are presented in Fig. 3 for various values of c. As c is increased, the degree of numerical dissipation also appears to increase. Of interest is the fact that when $c = c_-(3)/2$ the L^2 energy remains approximately constant, implying that negative values of c are able to counteract numerical dissipation of L^2 energy due to the upwind flux.

Finally, a plot of the solution at time $t = 1$ (for the case of a fully upwind interface flux) is presented in Fig. 4 for a scheme with $c \to \infty$. It can be seen that the Gaussian initial condition 'leaves behind' high order components as it is advected to the right (in line with the discussions presented in Sect. 3.6). This is clearly an undesirable property, resulting in a significant loss of accuracy as illustrated in Fig. 2(e).

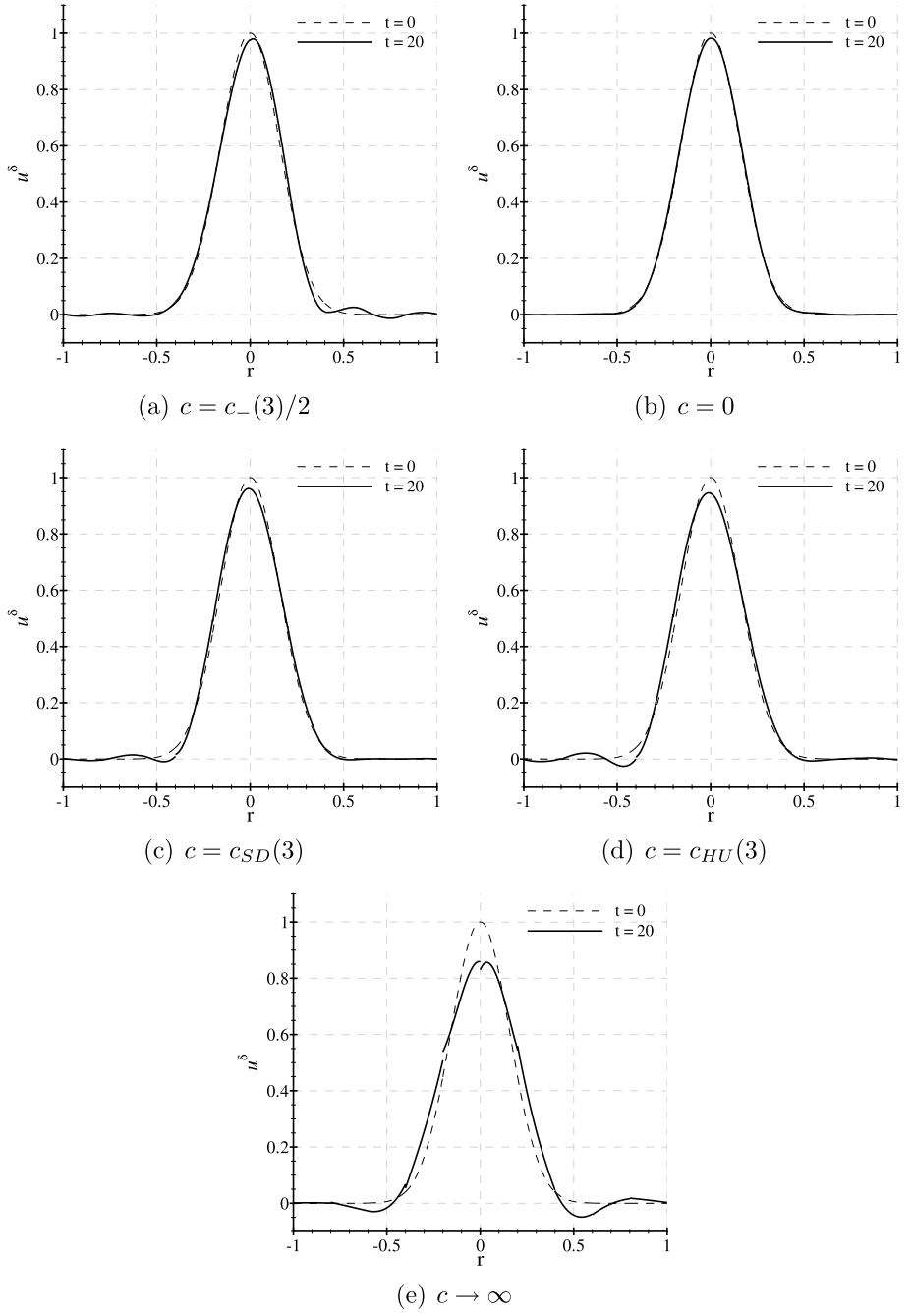

Fig. 2 Plots of solution to the linear advection equation at time $t = 20$ (*solid lines*) for schemes with $c = c_-(3)/2$ (**a**), $c = 0$ (**b**), $c = c_{SD}(3)$ (**c**), $c = c_{HU}(3)$ (**d**) and $c \to \infty$ (**e**). The Gaussian initial condition is shown as a *dashed line* in each plot. In all cases a fully upwind flux was prescribed between adjoining elements

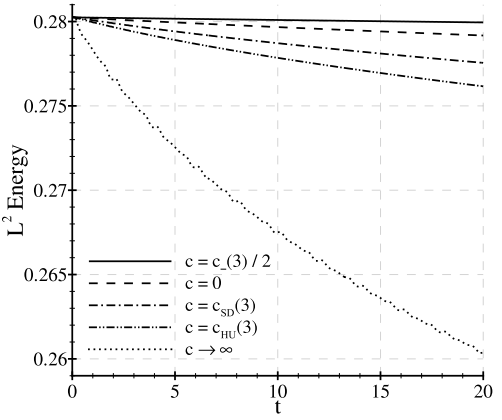

Fig. 3 Plots of L^2 energy against time for solutions of the linear advection equation. Various values of c are considered. In all cases a fully upwind flux was prescribed between adjoining elements

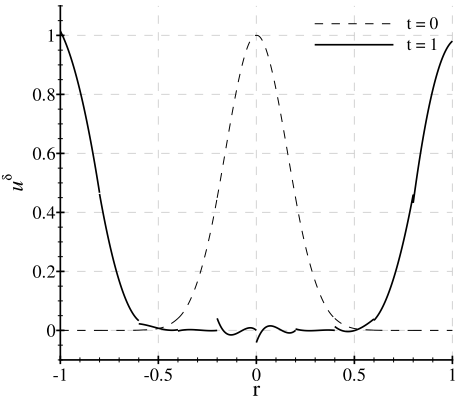

Fig. 4 Plot of the solution to the linear advection equation at time $t = 1$ (*solid line*) for a scheme with $c \to \infty$. The Gaussian initial condition is shown as a *dashed line*. A fully upwind flux was prescribed between adjoining elements

4.1.3 Results (Central Flux)

Plots of the solution at time $t = 20$ (for the case of a central interface flux) are presented in Fig. 5 for various values of c. As for the case of a fully upwind interface flux, the most accurate result is achieved when $c = 0$ (recovering a nodal DG scheme). When $c = c_-(3)/2$ oscillations are observed to form predominantly downwind of the Gaussian profile, and when $c = c_{SD}(3)$ and $c = c_{HU}(3)$ oscillations are observed to form both upwind and downwind of the Gaussian profile. In the limit $c \to \infty$ (plot not shown) the Gaussian profile is almost instantaneously destroyed as time begins to advance.

Plots illustrating how the L^2 energy of the solution varies with time (for the case of a central interface flux) are presented in Fig. 6 for various values of c. It can be seen that L^2 energy stays exactly constant when $c = 0$ (recovering a nodal DG scheme). When $c = c_-(3)/2$, $c = c_{SD}(3)$, and $c = c_{HU}(3)$ small amplitude oscillations of the L^2 energy are observed. For all cases (in which a central flux was prescribed between elements) it was found that the broken Sobolev norm $\|u^\delta\|_{k,2}$ remained exactly constant as time advanced. Such a result is in line with (3.18) for a central interface flux ($\kappa = 1$).

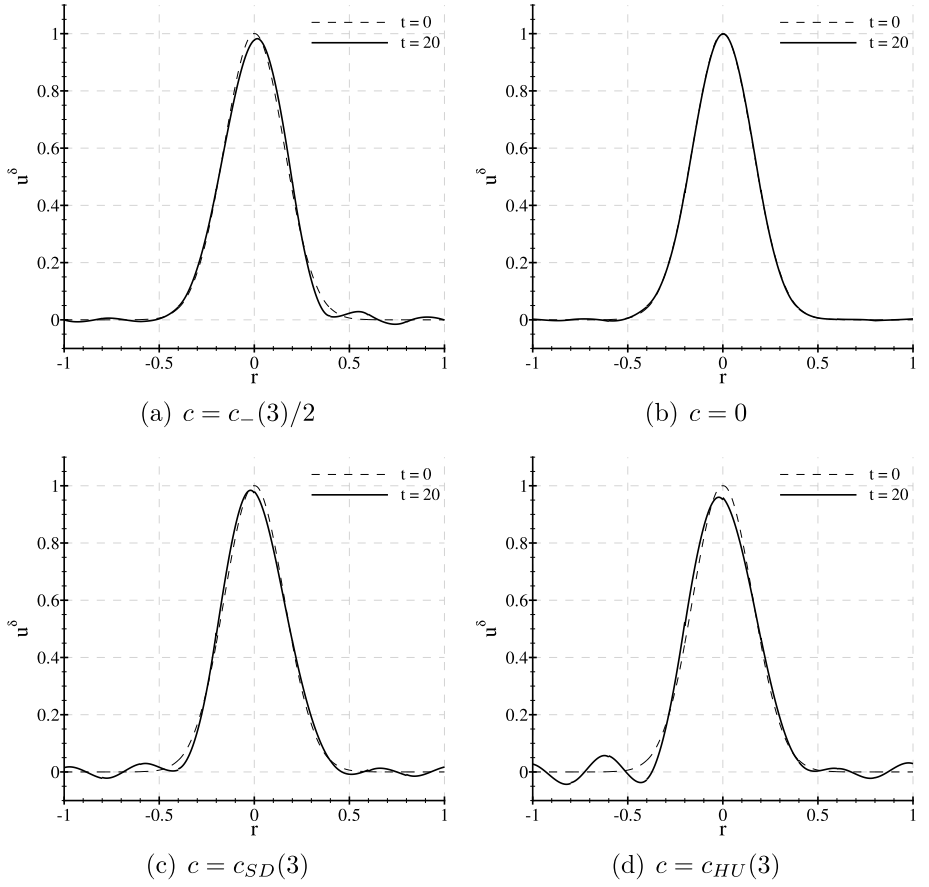

Fig. 5 Plots of solution to the linear advection equation at time $t = 20$ (*solid lines*) for schemes with $c = c_-(3)/2$ (**a**), $c = 0$ (**b**), $c = c_{SD}(3)$ (**c**) and $c = c_{HU}(3)$ (**d**). The Gaussian initial condition is shown as a *dashed line* in each plot. In all cases a central flux was prescribed between adjoining elements

4.2 Spatially Varying Flux

4.2.1 Overview

The stability analysis and numerical experiments presented thus far have been for cases where the flux function is linear. To be practically useful, however, energy stable FR schemes must also perform well when the flux is non-linear. One can gain insight into the non-linear performance of energy stable FR schemes by considering properties of the nodal DG scheme that is recovered when $c = 0$. As has been mentioned previously, the recovered scheme involves a collocation projection of the flux onto a polynomial space of degree k; using flux values at the $k + 1$ solution points. It can be shown that for a non-linear flux function such a collocation based nodal DG scheme suffers from aliasing-driven instabilities if the solution is under-resolved (for a detailed discussion see, for example, the textbook by Hesthaven and Warburton [4]). It is therefore reasonable to propose that, in general, energy stable FR schemes may suffer from aliasing driven instabilities when solving non-linear problems. In

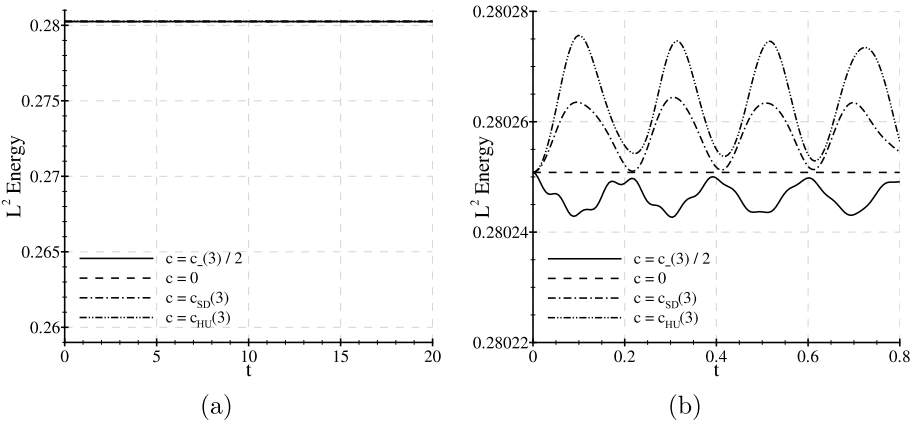

Fig. 6 Plots of L^2 energy against time for solutions of the linear advection equation are shown in (**a**). The same data within a reduced temporal range of $0 \leq t \leq 0.8$ is shown in (**b**). Various values of c are considered. In all cases a central flux was prescribed between adjoining elements

order to investigate the aforestated proposition, numerical experiments were carried out in which (2.1) was solved with the following flux function

$$f(x,t) = \left[(1-x^2)^5 + \frac{1}{2}\right] u(x,t). \tag{4.3}$$

Although such a flux is in fact linear in u, it is spatially dependent, and has been used previously (in the textbook of Hesthaven and Warburton, for example [4]) to investigate aliasing driven instabilities.

For all experiments the computational domain was defined to be $\mathbf{\Omega} = [-1, 1]$. Cases in which a central flux was prescribed between adjoining elements were considered ($\mathbf{\Omega}$ divided into 40 elements of equal size), and cases in which a fully upwind flux was prescribed between adjoining elements were also considered ($\mathbf{\Omega}$ divided into 30 elements of equal size). In all cases the solution was represented within each element by a third order polynomial, defined by solution values at four Gauss-Lobatto points. Periodic boundary conditions were applied at the ends of $\mathbf{\Omega}$, and the following initial condition was prescribed within $\mathbf{\Omega}$ at $t = 0$

$$u(x,0) = \sin(4\pi x). \tag{4.4}$$

Time integration was performed using an explicit five-stage low storage fourth-order Runge-Kutta scheme [15].

4.2.2 Results (Central Flux)

Plots of L^2 energy against time t (for the case of a central interface flux) are shown in Fig. 7 for various values of c. It can be seen that the nodal DG scheme ($c = 0$) is unstable. This is in line with the results obtained by Hesthaven and Warburton [4], and occurs due to aliasing-driven instabilities. In practice, such aliasing-driven instabilities are often remedied by application of a filter, applied repeatedly (at a computational cost) as the solution is advanced in time [4]. In contrast to the nodal DG method, it can be seen that the SD method, obtained when $c = c_{SD}(3)$, and the Huynh type method, obtained when $c = c_{HU}(3)$, are

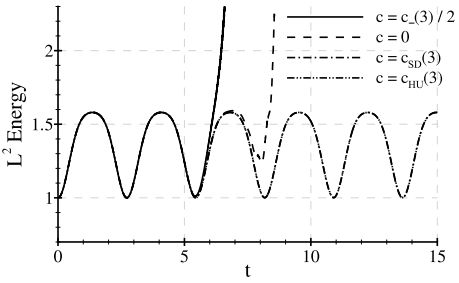

Fig. 7 Plots of L^2 energy against time for cases where the flux function is spatially varying; defined by (4.3). Results for various values of c are presented. In all cases a central flux was applied between adjoining elements

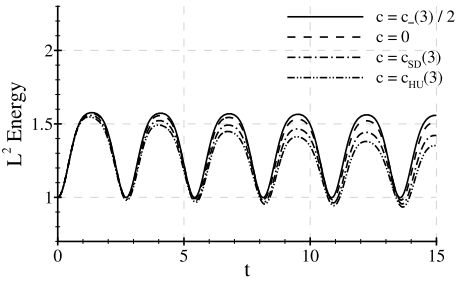

Fig. 8 Plots of L^2 energy against time for cases where the flux function is spatially varying; defined by (4.3). Results for various values of c are presented. In all cases a fully upwind flux was applied between adjoining elements

both stable. It appears that schemes based on positive values of c are able to damp aliasing-driven instabilities before they cause the solution to blow-up; without the need for any filter to be applied. Such a result implies that the SD method and the Huynh type method can be viewed as automatically 'filtered' nodal DG schemes. Finally, it can be noted that when $c = c_-(3)/2$ the resulting scheme is less stable than the nodal DG method ($c = 0$), blowing up at an earlier time.

4.2.3 Results (Fully Upwind Flux)

Plots of L^2 energy against time t (for the case of a fully upwind interface flux) are shown in Fig. 8 for various values of c. It is evident that all cases remain stable *i.e.* the use of a fully upwind interface flux damps the aliasing-driven instabilities present when a central flux is employed. It is also evident that numerical dissipation increases as c is increased.

4.3 Summary

The findings of the numerical experiments presented in this study suggest that:

- The most accurate results are obtained when $c = 0$ (recovering a nodal DG scheme).
- Increasing c increases numerical dissipation.
- Increasing c increases stability.
- A significant loss of accuracy occurs in the limit $c \to \infty$.

Additional more detailed studies are necessary in order to fully understand this behavior, and quantify exactly how both accuracy and stability of energy stable FR schemes depend on c.

5 Extension to Multiple Dimensions

The 1D energy stable schemes identified in this study can be extended to quadrilateral and hexahedral elements via the construction of tensor product bases as described by Huynh [12]. However, in simplex elements the direct construction of a tensor product basis is not possible, and one must use an alternative methodology to identify stable FR schemes. We are currently attempting to develop such an alternative methodology (based on the 1D approach presented in this study) in order to develop energy stable FR schemes on triangles.

6 Conclusions

A new class of high-order energy stable FR schemes has been identified. The schemes are parameterized by a single scalar quantity c, which if chosen judiciously leads to the recovery of several well known high-order methods (including a particular nodal DG method and a particular SD method), as well as one other FR scheme that was previously found by Huynh to be stable [12]. Preliminary numerical studies indicate that the most accurate results are obtained when $c = 0$ (recovering a nodal DG scheme). It is also found that increasing c leads to an increase in numerical dissipation, and thus additional stability. Of particular note is the fact that schemes with positive values of c appear to damp aliasing-driven instabilities which cause the nodal DG scheme ($c = 0$) to become unstable when the flux function varies spatially.

The analysis offers significant insight into why certain flux reconstruction schemes are stable, whereas others are not. Also, from a practical standpoint, the analysis provides a simple prescription for implementing an infinite range of energy stable high-order methods via the intuitive FR approach. Future studies should further investigate how both accuracy and stability of energy stable FR schemes depend on c, as well as ascertaining whether the 1D methodology presented here can be extended to develop energy stable FR schemes for simplex elements.

Acknowledgements The authors would like to thank the National Science Foundation (grant 0708071), the Air Force Office of Scientific Research (grant FA9550-07-1-0195), the National Sciences and Engineering Research Council of Canada and the Fonds de Recherche sur la Nature et les Technologies du Québec for supporting this work.

References

1. Reed, W.H., Hill, T.R.: Triangular mesh methods for the neutron transport equation. Technical Report LA-UR-73-479, Los Alamos National Laboratory, Los Alamos, New Mexico, USA (1973)
2. Cockburn, B., Shu, C.: Runge–Kutta discontinuous Galerkin methods for convection-dominated problems. J. Sci. Comput. **16**, 173 (2001)
3. Arnold, D.N., Brezzi, F., Cockburn, B., Marini, L.D.: Unified analysis of discontinuous Galerkin methods for elliptic problems. SIAM J. Numer. Anal. **39**, 1749 (2001)
4. Hesthaven, J.S., Warburton, T.: Nodal Discontinuous Galerkin Methods—Algorithms, Analysis, and Applications. Springer, Berlin (2008)
5. Hesthaven, J.S., Warburton, T.: Nodal high-order methods on unstructured grids. J. Comput. Phys. **181**, 186 (2002)
6. Giraldo, F.X., Hesthaven, J.S., Warburton, T.: Nodal high-order discontinuous Galerkin methods for the spherical shallow water equations. J. Comput. Phys. **181**, 499 (2002)
7. Kopriva, D.A., Kolias, J.H.: A conservative staggered-grid Chebyshev multidomain method for compressible flows. J. Comput. Phys. **125**, 244 (1996)

8. Liu, Y., Vinokur, M., Wang, Z.J.: Spectral difference method for unstructured grids I: basic formulation. J. Comput. Phys. **216**, 780 (2006)
9. Wang, Z.J., Liu, Y., May, G., Jameson, A.: Spectral difference method for unstructured grids II: extension to the Euler equations. J. Sci. Comput. **32**, 45 (2007)
10. Liang, C., Premasuthan, S., Jameson, A.: High-order accurate simulation of low-Mach laminar flow past two side-by-side cylinders using spectral difference method. Comput. Struct. **87**, 812 (2009)
11. Liang, C., Jameson, A., Wang, Z.J.: Spectral difference method for compressible flow on unstructured grids with mixed elements. J. Comput. Phys. **228**, 2847 (2009)
12. Huynh, H.T.: A flux reconstruction approach to high-order schemes including discontinuous Galerkin methods. In: AIAA Computational Fluid Dynamics Meeting (2007)
13. Jameson, A.: A proof of the stability of the spectral difference method for all orders of accuracy. J. Sci. Comput. **45**(1–3), 348–358 (2010)
14. Roe, P.L.: Approximate Riemann solvers, parameter vectors, and difference schemes. J. Comput. Phys. **43**, 357 (1981)
15. Carpenter, M.H., Kennedy, C.: Fourth-order 2N-storage Runge-Kutta schemes. Technical Report TM 109112, NASA, NASA Langley Research Center (1994)